a *D* mechanism for Tm and Yb, and a mechanistic crossover occurs at Er.

Acknowledgment. The authors express their thanks to R. Ith, P. Pollien, and R. Tschanz for their machine work in the construction of the high-pressure probe-heads and for their valuable suggestions regarding design. This work was supported by the Swiss National Science Foundation under grand 2.256-0-81.

Registry No. DMF, 68-12-2; $Ce(DMF)_8^{3+}$, 45316-14-1; $Pr(DMF)_8^{3+}$, 45316-20-9; $Nd(DMF)_8^{3+}$, 45316-19-6; $Tb(DMF)_8^{3+}$, 51232-27-0; $Dy(DMF)_8^{3+}$, 51223-48-4; $Ho(DMF)_8^{3+}$, 51232-29-2; $Er(DMF)_8^{3+}$, 51232-31-6; $Tm(DMF)_8^{3+}$, 51232-33-8; $Yb(DMF)_8^{3+}$, 51232-35-0; ^{17}O, 13968-48-4.

Supplementary Material Available: Experimental data for the temperature and pressure dependence of pure DMF (Table SI) and $Ln(ClO_4)_3$ solutions (Tables SII to SVII), formyl proton relaxation rates, and chemical shifts; detailed results and correlation coefficient matrix of the least-squares analysis of NMR data (Table SVIII); experimental data for the variable temperature and pressure study of Nd^{3+} by spectrophotometry (Table SIX) (31 pages). Ordering information is given on any current masthead page.

Surface Spectroscopic Studies of Polymer Surfaces and Interfaces: Poly(tetramethyl-*p*-silphenylenesiloxane)

Joseph A. Gardella, Jr.,*† J. S. Chen,‡ J. H. Magill,‡ and David M. Hercules*

Contribution from the Departments of Chemistry and Metallurgical and Materials Engineering, University of Pittsburgh, Pittsburgh, Pennsylvania 15260. *Received August 5, 1982*

Abstract: Surface spectroscopic (ESCA, FTIR) studies of changes in the morphology of fractionated poly(TMpS) solution-grown crystal mats (I), melt-cast mats (II), melt-quenched mats (III), and solution-cast films (IV) have been correlated with thermal (differential scanning calorimetry), crystallographic (small angle X-ray scattering), and gas phase (HF) reaction studies. These results provide a complete picture of the surface structure of this well-ordered macromolecular material, demonstrating for the first time the use of ESCA to analyze the morphology of an ordered homopolymer. ESCA analyses of various degrees of crystallinity of poly(TMpS) (I > II > III > IV) were correlated with FTIR results yielding the conclusion that the surface (amorphous) region of each material consists of surface-segregated Si-C_6H_4-Si-O linkages, most likely in the form of folds or loops of the long chains back into the rod-like crystalline core of the materials. Chemical etching studies were accomplished with gaseous HF (diluted with He 10:30 v/v) which selectively reacts with and removes the less-ordered surface amorphous regions, thereby increasing the overall crystallinity. This process was followed both spectroscopically and with DSC and SAXS analysis, providing results which demonstrate the efficacy of these methods and confirm the surface chemistry and morphology of the polymer system.

Introduction

Elucidation of structure–property relationships in polymeric materials is a goal of much research which is intent on development of property specificity in polymers. Chemical structure at the monomer level and in the polymer chain itself have been shown to be important determinants of various physical properties. The study of ordered or crystalline polymers constitutes one important aspect of these studies.

Since Palmer and Cobbald[1] first discovered that warm, concentrated nitric acid preferentially attacks the less-ordered regions in polyethylene (PE), chemical degradation studies have been conducted to probe the morphology of crystalline polymers. For instance, investigations by Peterlin and Meinel[2] and Priest and Keller[3] on polyethylene, isotactic polypropylene by Hock,[4] and cellulose by Manley[5] have shown that structure–property relationships may be obtained by using chemical degradation as a structural probe. More recent work on crystalline polyethylene[6,7] has provided information on the morphology of polyethylene single crystals.

Spectroscopic analysis is common for deducing polymer structure.[8] Recently, Fourier transform infrared spectroscopy (FTIR) has been used, especially for studying polymer morphology of crystalline polyethylene.[9-11] Advantages such as high spectral resolution, reproducibility in band position and intensity, signal to noise enhancement, and data processing capabilities have made FTIR one of the most suitable techniques for studying the relatively small spectral changes associated with polymer morphology and corresponding crystallinity features. X-ray photoelectron spectroscopy (XPS or ESCA) has also been used extensively in the analysis of the chemical structure of polymers.[12,13] ESCA is sensitive to surface structure (10–50 Å) and compares favorably with other surface spectroscopic measurements[14] in its ability to distinguish between structural differences in homopolymers. However, it frequently lacks definitive interpretation when utilized alone. For this reason, it is best to use ESCA with other spec-

* Department of Chemistry.
† Department of Chemistry, State University of New York at Buffalo, Buffalo, NY 14214.
‡ Department of Metallurgical and Materials Engineering.

(1) Palmer, R. P.; Cobbald, A. *Macromol. Chem.* **1964**, *74*, 174.
(2) Peterlin, A.; Meinel, G. *J. Polym. Sci., Part B* **1965**, *3*, 9.
(3) Priest, D. J. *J. Polym. Sci. Part A2* **1971**, *9*, 1777; Keller, A.; Priest, D. J. *J. Macromol. Sci. (B)* **1968**, *2*, 479.
(4) Hock, W. W. *J. Polym. Sci. Phys.* **1965**, *3*, 573; *J. Polym. Sci., Part A2*, **1966**, *4*, 227.
(5) Manley, R. St. J. *J. Polym. Sci. Polym. Phys. Ed.* **1974**, *12*, 1347.
(6) Keller, A.; Martuscelli, E.; Priest, d. J.; Udagawa, Y. *J. Polym. Sci., Part A* **1971**, *9*, 1807.
(7) Patel, G. N.; Keller, A. *J. Polym. Sci. Polym. Phys. Ed.* **1975**, *13*, 22.
(8) Hummel, D. O. "Infrared Analysis of Polymers, Resins and Additives, An Atlas"; Wiley-Interscience: New York, 1971.
(9) Painter, P. C.; Havens, J.; Hart, W. W.; Koenig, J. L. *J. Polym. Sci., Polym. Phys. Ed.* **1977**, *15*, 1223.
(10) Bank, M. I.; Krimm, S. *J. Polym. Sci. Part A2* **1969**, *7*, 1785.
(11) Ching, J. H. C.; Krimm, S. *J. Appl. Phys.* **1975**, *46*, 4181.
(12) Clark, D. T. "Handbook of X-ray and Ultraviolet Photoelectron Spectroscopy"; D. Briggs, Ed.; Heyden: London, 1972; pp 211-247.
(13) Dwight, D. W. "Photon, Electron and Ion Probes of Polymer Structures and Properties"; Dwight, D. W.; Fabish, T. J.; Thomas, H. R., Ed.; American Chemical Society: Washington, DC, 1981.
(14) Gardella, J. A., Jr.; Hercules, D. M. *Anal. Chem.* **1981**, *53*, 1879.

0002-7863/83/1505-4536$01.50/0

troscopic measurements to verify and complement the ESCA results.[14,15]

The present investigation combines spectroscopic, calorimetric, and X-ray measurements with chemical or surface degradation studies to ascertain the location and degree of order (or disorder) in a crystalline polymer system. Specifically, poly(tetramethyl-*p*-silphenylenesiloxane) [poly(TMpS)] is investigated, because previous work has shown that the less-ordered regions of single crystals of this polymer are located primarily at the surfaces.[16] Published results utilizing selective surface degradation indicate that 48% HF solution at 30 °C[16-18] primarily affects siloxane bond cleavage at crystal surfaces.

Crystallinity of poly(TMpS) was determined by differential scanning calorimetry (DSC)[17] and was related to earlier X-ray work, in which it was found that poly(TMpS) can attain a higher degree of crystallinity after etching with HF solution.[17]

Utilization of surface sensitive probes like ESCA and FTIR enables one to study the surface morphology of poly(TMpS) where the "core" material is highly crystalline. Differential scanning calorimetry (DSC) and small-angle X-ray scattering (SAXS) measurements provide important supplementary morphological results which follow surface chemical etching. Direct spectroscopic characterization can relate reactivity with structure, for example, the lower reactivity of the ordered crystalline core and the higher reactivity of the less-ordered surface. Such correlations can form the basis for other studies arrived at improving our understanding of the role of polymer morphology in developing materials for specific uses.[19] The significance of polymeric interfaces vis à vis physical and engineering properties is a case in point.

Experimental Section

A. Polymer Materials and Preparation. Previous work[16-19,21-23] described the synthesis and characterization of fractionated poly(TMpS). The homopolymer was fabricated in different material forms and fractionated. These forms were: (I) single-crystal mats ($\bar{M}_v = 3.38 \times 10^4$ daltons), (II) melt-cast mats ($\bar{M}_v = 3.38 \times 1/^4$ daltons), (III) melt-quenched mats ($\bar{M}_v = 3.38 \times 10^4$ daltons), and (IV) solution-cast films ($\bar{M}_v = 1.97 \times 10^5$ daltons).

(I) Single Crystals. Solution-grown crystals (I) of poly(TMpS) were made by the well-known self-seeding procedure generally used for growing single crystals.[20,21] The poly(TMpS) crystals in this study were precipitated at 28 °C from 2:1 (v/v) benzene–methanol at a concentration of 0.05 wt % according to established procedures.[10] Polymer single crystals were precipitated from this dilute solution and allowed to settle slowly onto cleaned flat platinum foil strips. The solvent was carefully removed and the samples were further dried at room temperature for several days before study. The overall sample integrity was checked by scanning electron microscopy (SEM), with a type AMR 200 instrument which provided an extensive overview of large areas of sedimented single crystals. The morphology of these solution-grown poly(TMpS) crystals has already been examined by transmission electron microscopy (TEM).[21,22]

(II) Melt-Cast Mats. Samples of poly(TMpS) single-crystal mats (II) were melted at 160 °C for 10 min on platinum strips and then cooled to room temperature. The observed melting of these crystals occurs just above 130 °C.

(III) Melt-Quenched Mats. Samples of poly(TMpS) single-crystal mats were melted on aluminum foil for 10 min at 160 °C, followed by rapid quenching in liquid N_2. After the samples were allowed to warm up to room temperature (above the polymer glass transition temperature of p(TMpS) (−22 °C)), they recrystallized.

(IV) Solution-Cast Film. Bulk polymer was prepared as a thin film (IV) by solution casting of the polymer in spherulitic form from benzene/methanol. Afterwards the specimens were allowed to dry in air and then in vacuum.

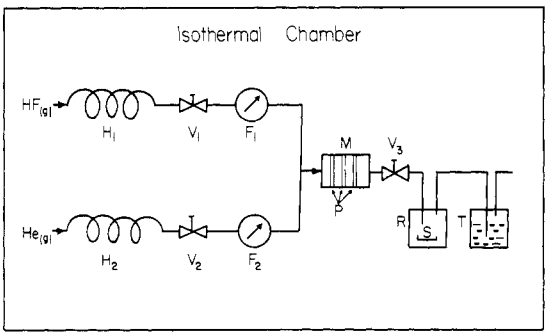

Figure 1. Diagram of monel flow reaction system. Components H_1 and H_2 are heat exchangers, V_1, V_2, and V_3 are control valves, F_1 and F_2 are flow meters, M is a mixer, P is perforated disks, R is the reaction cell, S is the polymer sample, and T is a trap. All components are monel metal except for R (polyethylene).

B. Sample Treatments. The entire etching apparatus, shown in Figure 1, was thermostated in a heated chamber at 45 °C. Incoming gases, HF and He, were rapidly equilibrated to this temperature on passage through coils (heat exchangers H_1 and H_2) before entering the mixer, M. The system was made of Monel metal, except for a polyethylene vessel which housed the poly(TMpS) specimen. For chemical etching a homogeneous mixture of carefully monitored preheated HF(g) and He(g) was passed over the polymer sample. A 10:30 (v/v) mixture of HF/He at 45 °C, at a total flow rate of 40 cm^3/min was used at various exposure times from 5 to 30 min duration in the current work. After many trials with different mixtures and flow rates, these conditions were established as suitable for monitoring the degradation of poly(TMpS) without causing serious sample deterioration. Following degradation the specimen was placed under vacuum for several hours at room temperature before spectroscopic or other measurements were performed.

C. Crystallinity Measurements. A Perkin-Elmer differential scanning calorimeter (DSC-2) with scanning auto zero and computer accessories was used to obtain heats of fusion (ΔH_f) of the poly(TMpS) samples initially and after different degrees of etching. A calorimetric sensitivity of 2 mcal/s and a heating rate of 20 °C/min were used. The DSC was calibrated with indium ($\Delta H_f = 6.8$ cal/g) and other high-purity metals according to established procedures. The heats of fusion of etched and unetched poly(TMpS) were converted to percentage crystallinities based on 13 cal/g as the ΔH_f of 100% crystalline poly(TMpS).[17]

D. Small-Angle X-Ray Diffraction (SAXS). The thicknesses of the single crystal specimens, before and during various stages of surface degradation, were measured using a Rigaku-Denki small-angle X-ray camera and a 6-kW rotating anode X-ray generator. Cu Kα radiation was used as the X-ray source, and diffraction patterns were recorded photographically following established procedures.[17,19]

E. Spectroscopic Analysis. Fourier transform infrared-attenuated total reflectance (FTIR/ATR) was used to analyze the poly(TMpS) specimens supported on platinum foils. Spectra were recorded with a Digilab FTS-10 M single-beam spectrometer coupled with a Data General Nova II minicomputer with a Harrick 4x beam condenser, set at 60° for ATR analysis.[24] A high signal-to-noise ratio was obtained by taking 500 scans of the specimen and 100 scans of the reference. A resolution of 4 cm^{-1} was used throughout the study.

ESCA spectra were recorded with a Hewlett-Packard HP 5950 A spectrometer fitted with an HP 5952 System III data system. The spectrometer was modified with a Surface Science Laboratories Model 234 imaging detector and a Model 224 aperture control. An ultrahigh vacuum preparation chamber, with a Leybold-Heraeus 360 L/s turbomolecular pump was used for preliminary pumpdown of samples, before their introduction into the analysis chamber. The time needed to reach the 10^{-9} torr range was typically 10–30 min. The analysis chamber was kept in the 10^{-10} torr range continuously. For analysis, monochromatic Al Kα radiation was used (1486.8 eV with resolution = 0.8 eV on Au $4f_{7/2}$ line) as the excitation source, with the aperture closed. Multiple scans (typically 120) were averaged for each 10- or 20-eV region (256 channels/region), which were scanned consecutively. Wide scans (1000 eV) were taken initially to check for contamination. Checking the intensities and peak shapes at 10-min intervals indicated no change with time due to heating or X-ray exposure during a typical run. A flood gun (1.0 eV, 0.4 mA) was used for charge compensation.

(15) Hercules, D. M. *Anal. Chem.* **1978**, *50*, 739A.
(16) Okui, N.; Magill, J. H.; Gardner, K. H. *J. Appl. Phys.* **1977**, *48*, 4116.
(17) Okui, N.; Li, H. M.; Magill, J. H. *Polymer* **1977**, *18*, 1152; **1978**, *19*, 411.
(18) Magill, J. H. "Treatise on Materials Science and Technology; Volume 10, Properties of Solid Polymeric Materials, Part 10 A"; J. M. Schultz, Ed.; Academic Press: New York, 1977; pp 3–368.
(19) Pollack, S. S.; Magill, J. H. *J. Polym. Sci., Part A2* **1969**, *7*, 551.
(20) Blundell, J.; Keller, A.; Kovacs, A. J. *J. Polym. Sci. Part B* **1966**, *4*, 481.
(21) Kojima, J.; Magill, J. H.; Merker, R. L. *J. Polym. Sci.* **1974**, *12*, 317; Haller, M. N.; Magill, J. H. *J. Appl. Phys.* **1969**, *40*, 4261.
(22) Gardner, K. H.; Magill, J. H.; Atkins, E. D. T. *Polymer* **1978**, *19*, 370.
(23) Li, H. M.; Magill, J. H. *Polymer* **1978**, *19*, 416.
(24) Harrick, N. J. "Internal Reflectance Spectroscopy"; Wiley-Interscience: New York, 1967.

Table I. Crystallinity Results for Poly(TMpS) Forms from Differential Scanning Calorimetry

form	ΔH_f, cal/g	% crystallinity[a]
solution-cast films (IV)	6.0	46
melt-quenched mats (III)	6.4	49
melt-cast mats (II)	7.6	58
single-crystal mats (I)	10.8	83

[a] Calculated from ΔH_f; see text. Relative standard deviation ±5%.

Table II. Infrared Absorption Bands for poly(TMpS) (4000–500 cm^{-1})

cm^{-1}	intensity[a]	assignments
3022	w	PhH, C-H stretching[25]
2975	w	$Si(CH_3)_2$, CH_3 asymmetric mode[25]
1258	sh	$Si(CH_3)_2$, CH_3 rocking mode[25]
1251	s	$Si(CH_3)_2$, CH_3 rocking mode[25]
1138	s	Si-O-Si stretch[26]
1075	vs	Si-O-Si stretch[26]
1020	sh	PhH, C-H band on Ph
880	wsh	Si-O hydroxy stretch[32]
1030, 800	w	Si-F stretching[33]
825	ssh	Si-C stretching[27]
780	vs	Si-C symmetric bend[25]
735	sh	PhH out of plane bending of H[24]
695	w	PhH[24]
635	vw	Si-O-Si + δ_1[25]
500	m	Si-O-Si symmetric bend[28]

[a] s, strong; m, medium; w, weak; v, very; sh, shoulder.

Results

This section will be treated in two parts: (A) calibration of the spectroscopic analysis of crystallinity by various untreated poly(TMpS) samples and (B) determination of the gas-phase reaction effects by spectroscopy and thermal and SAXS analysis. The first part serves to demonstrate the capabilities of ESCA, compared with the more established FTIR/ATR technique. The second part utilizes the spectroscopic methods as direct probes of the surface chemistry and morphological changes which are effected by gas-phase etching. These spectroscopic measurements are supported by the same thermal and SAXS measurements used for calibration. All studies serve to elucidate the surface structure and morphology of this system while describing structure-related reactivities which serve as a first step in property specific polymer structure development.

A. Calibration. Crystallinities from DSC measurements of the various samples of poly(TMpS) are given in Table I. The heat of fusion (ΔH_f) of each specimen was converted to percentage crystallinity by using 13 cal/g as the 100% crystallinity level of poly(TMpS).[17] The solution-grown single crystals (I) have the highest crystallinity, followed by the melt-cast (II), melt-quenched (III), and solution-cast film (IV). For the film (IV), the lower crystallinity derives in part from the higher molecular weight of IV compared to I, II, and III. These samples are utilized to calibrate the spectroscopic methods, illustrating the type and range of information which can be obtained from ESCA and FTIR–ATR, while providing a reference base for the etching studies.

Results of the FTIR–ATR analysis of I–IV are given in Table II.[25–33] The ATR infrared mode was chosen for analysis because

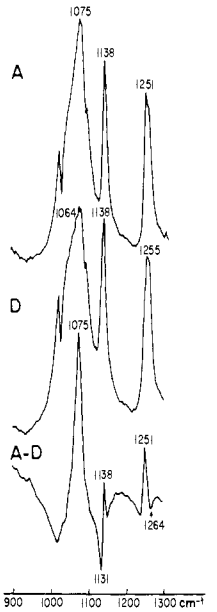

Figure 2. FTIR–ATR spectra: (A) poly(TMpS) single-crystal mats (I); (D) poly(TMpS) melt-quenched mats (III); (A–D) difference spectrum (1:1) showing critical bands and crystallinity changes between samples. Details are listed in Table II.

of the high scattering exhibited by the crystals which complicated conventional transmission spectra. In addition, ATR is more sensitive to the surface of the samples[24] than transmission spectroscopy, which would average results of structure from the entire polymer. However, the sampling depth of the FTIR–ATR method is sufficient to average several layers of crystals (150–2000 Å).[24] Differences between the forms are illustrated by spectral subtraction in Figure 2. The most significant spectral differences between the samples are found in the bands near 1251 cm^{-1} ($Si-CH_3$ rock), 1138 cm^{-1}, and 1075 cm^{-1} (siloxane Si–O–Si stretch). As specimen crystallinity decreases, the intensity of the sharp 1251-cm^{-1} peak also decreases. This band tends to shift to 1255 cm^{-1} and broadens as one proceeds from the single-crystal to the solution-cast film. This is illustrated dramatically in the difference spectrum in Figure 2 where a 1:1 subtraction of the single-crystal (I) and the melt-quenched samples (III) exhibits a positive band at 1251 cm^{-1}. This result correlates with previous work which analyzed molten p(TMpS)[29] by FTIR. No band at 1251 cm^{-1} was observed.

A similar shift is seen for the siloxane stretch bands located at 1138 cm^{-1}. Also, the peak at 1075 cm^{-1}, which is sharp and distinctive in the crystal spectrum, at first decreases in intensity and then broadens with a shift to lower frequencies for the melt-cast specimens of lower crystallinity. Figure 2 highlights all these features in the difference spectrum. The difference spectrum exhibits positive peaks at 1138 and 1075 cm^{-1} and negative features due to broadening of the 1131- and 1064-cm^{-1} bands. It is believed that the sharp infrared bands at 1251, 1138, and 1075 cm^{-1} are due to crystalline $Si-CH_3$ and Si–O–Si bands, and that the less crystalline material is responsible for broadening of these bands and shifts to 1255, 1131, and 1064 cm^{-1}, respectively, which are apparent in the difference spectra.

ESCA can be used to monitor morphological differences by following changes in surface composition;[13,30] previous results have been concerned with polymer blends and mixtures of different components, where one component segregates to the surface preferentially. It is often said that the ESCA technique samples deeply enough (10–50 Å) to yield results which accurately reflect

(25) Lady, J. H.; Bower, G. M.; Adams, R. E.; Byrne, F. P. *Anal. Chem.* **1959**, *3*, 1100.
(26) Ishida, H.; Koenig, J. L. *J. Polym. Sci. Polym. Phys. Ed.* **1980**, *18*, 233.
(27) Burger, H.; Sawodny, W. *Spectrochim. Acta* **1967**, *23A*, 2827.
(28) Lazarev, A. N. "Vibrational Spectra and Structure of Silicates"; Consultants Bureau: New York, 1972.
(29) Pingatore, W.; Magill, J. H., unpublished results.
(30) Knutson, K.; Lyman, D. J. In "Biomedical and Dental Applicators of Polymers"; Gebelein, E.; Koblitz, F. F., Ed.; Plenum: New York, 1981; p 173.
(31) Clark, D. T.; Thomas, H. R. *J. Polym. Sci., Polym. Chem. Ed.* **1976**, *14*, 1761.
(32) Gardella, J. A., Jr.; Hercules, D. M.; Magill, J. H., unpublished results.
(33) Ishida, H.; Koenig, J. L. *J. Polym. Sci. Polym. Phys. Ed.* **1980**, *18*, 233.

Table III. ESCA Binding Energies for Untreated Poly(TMpS)[a] (±0.1 eV)

sample	C 1s (fwhm)[b]	C (shake up)	O 1s (fwhm)[c]	Si 2p (fwhm)[c]	Si 2s[c]
single-crystal mats (I)	285.0(1.55)	291.5	532.5(1.38)	101.9(1.45)	153.2
melt-cast mats (II) and melt-quenched mats (III)	285.0(1.38)	291.5	532.5(1.38)	101.9(1.43)	153.1
solution-cast films (IV)	285.0(1.32)	291.5	532.5(1.70)	102.0(1.42)	153.2

[a] Referenced to C 1s at 285.0 eV for (CH_x). [b] Full width at half maximum in eV. [c] In addition, shake-up features for the O 1s, Si 2p, and Si 2s peaks were observed at 6.5 eV higher binding energy.

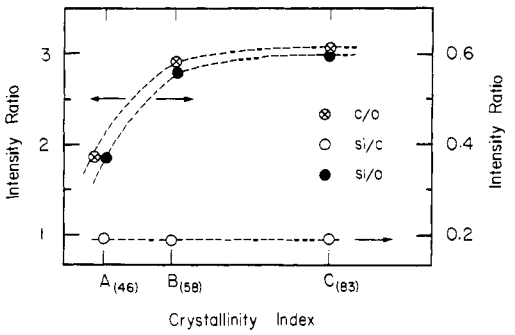

Figure 3. Plots of ESCA intensity ratios against crystallinity index for poly(TMpS): $A_{(46)}$, solution-cast films; $B_{(58)}$, melt-cast mats; $C_{(83)}$, single-crystal mats (number in brackets indicates crystallinity index). Basic information is given in Table I.

the bulk composition of homopolymers.[12-14,31] However, this is related to the amorphous nature of the structure of homopolymers under investigation. If a different morphology causes the structure of the top surface layers to differ from the bulk core, ESCA has the capability to detect it. In the present work, it is clearly shown that the topological changes encountered especially in the crystal (I) are paralleled by chemical changes monitored by ESCA.

ESCA binding energies for the poly(TMpS) samples are listed in Table III. Qualitatively, the ESCA results show only small differences between different sample forms, except perhaps for a tendency towards line-broadening in the more highly crystalline samples as judged from the FWHM values. However, the quantitative ESCA data in Figure 3 are very significant and are in accord with the FTIR data discussed above. Figure 3 indicates that as sample crystallinity increases in poly(TMpS), the surface oxygen content decreases, since the C/O and Si/O ratios increase in a similar fashion. However, the Si/C values remain constant as would be expected for decreasing surface oxygen. In considering the topological structure proposed for crystalline poly(TMpS),[17-19,21,22] the surface morphology may be based on the bonding characteristics of the monomer unit. Since the polymer crystal surface is presumed to be comprised of loops or folds where the disorder is greater than that found in the crystalline core material, consequently, the surface or interface comprises the least crystalline part of the polymer specimen.

The ESCA measurements clearly indicate that considerably more surface oxygen is present in poly(TMpS) samples of lower crystallinity, implying that a higher concentration of Si–O is found at the interfacial folds or loops of spherulitic lamellae. The surface sensitivity of ESCA with its 10–50 Å sampling depth[12] is much better than for FTIR (150–5000 Å).[24] Still, our vibrational results indicate that siloxane bonding (broadening and shifting) changes with trends or shifts toward higher crystallinity associated with a changing surface morphology. Subsequently, we are now able to utilize these spectroscopic tools in the direct analysis of selective surface degradation, since they provide direct confirmation of changes in surface morphology.

B. Degradation Studies. Previous work[6] has shown that selective chemical etching of crystalline poly(TMpS) by HF solution brought about an increase in relative sample crystallinity by preferentially etching away less ordered surface material. Early in the present work, spectroscopic characterization of an etched sample was found to be complicated due to considerable hydrolysis that occurred in HF solution.[29] However, with dry gaseous HF

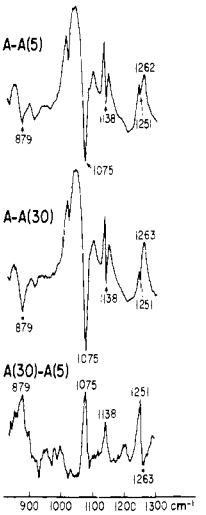

Figure 4. FTIR-ATR difference spectra: A-A(5), single-crystal mats, 5 min etched single-crystal mats (1:1); A-A(30), single-crystal mats, 30 min etching single-crystal mats; A(30)-A(15), 30 min etched single-crystal mats, 5 min etched single-crystal mats; (sample molecular weight fraction = 3.38×10^4).

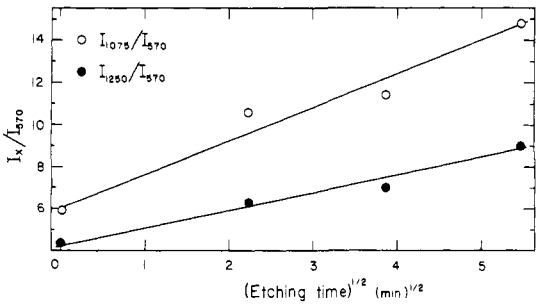

Figure 5. Plots of relative infrared peak intensities vs. etching time for poly(TMpS) crystal mats. Spectral details are given in Table II.

etching, spectroscopic monitoring of the chemical changes occurring on the crystal surface can be successfully employed to follow the etching process.

Figure 4 shows the FTIR difference spectra obtained for the crystal etching experiments. In obtaining these spectra, attention was focused on the bands at 1251 and 1075 cm^{-1}, which are associated with crystallinity. The ATR difference spectra obtained with a 1:1 subtraction of the untreated polymer from the poly(TMpS) crystal etched for different times are shown in Figure 4 (top and middle); note that negative peaks are apparent for the 1251 and 1075-cm^{-1} bands due to the subtraction. A plot of the relative intensities of the FTIR bands vs. etching time in Figure 5 reveals that an increase in intensity of the 1075- and 1251-cm^{-1} bands occurs with etching time. This result is in agreement with the difference spectra in Figure 4 (bottom), where a progressive increase in relative intensity for the crystallinity bands (1075 and 1251 cm^{-1}) is apparent for etching times on the order of 5–30 min.

The HF etching experiments also were followed by ESCA. The quantitative ESCA results reflect the calibration studies presented in Table III. The most significant differences is the gradual growth in intensity of a peak at 687.2 eV which can be assigned to the fluorine 1s peak. Examination of the other core levels (C 1s, Si

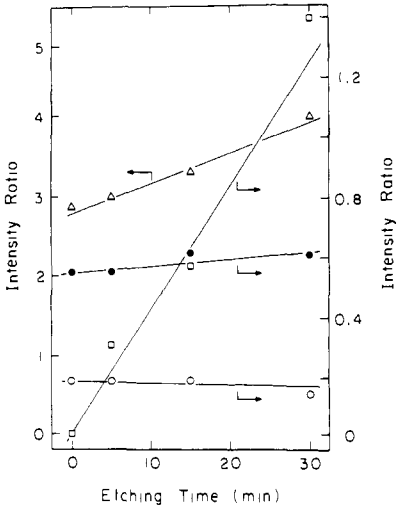

Figure 6. Plot of ESCA intensity ratios against etching time for poly(TMpS) melt cast mats; molecular weight fraction = 3.38×10^4: (○) Si/C; (●) Si/O; (△) C/O; (□) F/Si.

Table IV. ESCA Intensity Ratios for poly(TMpS) $HF_{(g)}$ Etching Experiments

sample form	etching time, min 0	5	15	30
(a) Single Crystal (I)				
C/O	3.06	3.17	3.54	3.37
Si, 2p/O	0.61	0.60	0.63	0.64
Si, 2p/C	0.199	0.190	0.178	0.189
F/C	0.0	0.039	0.159	0.141
F/O	0.0	0.121	0.565	0.494
F/Si	0.0	0.206	0.897	0.775
(b) Melt Cast Film (II)				
C/O	2.88	3.00	3.33	4.02
Si, 2p/O	0.55	0.55	0.62	0.61
Si, 2p/C	0.90	0.185	0.187	0.152
F/C	0.0	0.056	0.106	0.200
F/O	0.0	0.169	0.354	0.803
F/Si	0.0	0.305	0.570	1.32

2p, and O 1s) showed no obvious new features (peaks, shoulders, or broadening) which could be assigned to C–F, Si–F, or O–F bond formation. Comparison with standards for the fluorine 1s line[13] suggested that Si–F would be the most reasonable possibility of the three for bonding. The appearance and growth of a band due to Si–OH stretching at 880 cm^{-1} [34] was noted in the FTIR spectra in Figure 4. Previous work[16-19,21,22] suggests an etching mechanism of HF addition across Si–O–Si linkages to form Si–F and Si–OH. Thus, the FTIR data provided support for the Si–F assignment. The lack of a peak in the C 1s region due to C–F at 292.0 eV was especially important since chemical shifts for CF features are very large, allowing for resolution of individual peaks,[12,13] whereas shifts in the Si 2p and O 1s regions are not as large.[13,35,36]

The quantitative ESCA results shown in Figure 6 and Table IV were used to follow the extent of the etching reaction. The data in Table IV show that as the crystals and film are etched, the C/O and Si/O ratios increase, while the Si/C ratio remains constant. These results map the increase in crystallinity which is occurring as the more reactive amorphous surface Si–O–Si linkages are etched away, leaving the rod-like array of crystalline core chains. In the single-crystal samples, the ESCA results plateaued above 15 min of etching. This arises because there is less amorphous material present in single-crystal mats than there

(34) Smith, A. L. "Analysis of Silicones"; Wiley: New York, 1974.
(35) Monroe-Snider, A.; Magill, J. H., unpublished results.
(36) Gardella, J. A., Jr.; Hercules, D. M., unpublished results.

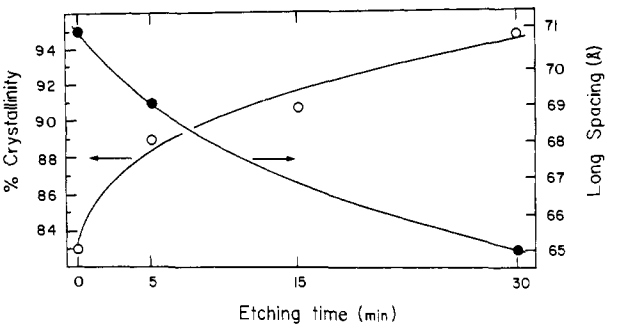

Figure 7. Plot of the degree of crystallinity and long spacing (Å) against etching time (min); single-crystal sample (I); for HF:He = 10:90 vol % at 45 °C: (○) % crystallinity; (●) long spacing.

is in the spherulitic films of lower crystallinity (i.e., samples A and B in Figure 3), which exhibit steady growth of crystallinity over the 30-min reaction period. These results are confirmed by the pattern of the fluorine uptake, shown by the F/Si ratio.

A final data set is given in Figure 7, where crystal stem lengths determined by SAXS measurements and by relative crystallinity (from DSC measurements) are plotted vs. etching time for the single-crystal sample (I). The SAXS periodicity, a measure of crystal thickness, is found to decrease as crystallinity increases during the etching process. These data support the proposed crystal etching model since the selective scission of Si–O–Si surface folds would effectively decrease the thickness. If etching were not surface (i.e., amorphous) selective, crystallinity would not increase and the crystal thickness would not change along the chain direction. The crystallinity reaches a maximum of 94% for the 30-min process; slightly higher levels have been achieved for HF solution etching experiments.[17]

Discussion

A. Calibration Studies. The calibration results present a consistent picture, demonstrating the utility of a multitechnique approach to surface analysis,[14] especially for a complex macromolecular system. In particular, the data confirm the model of Si–C_6H_4–Si–O bonds comprising surface linkages, since the amorphous regions of each sample can be assigned this structure from the changes in siloxane bonding exhibited by the shifts in vibrational band position (Figure 2). This is confirmed by the ESCA results (Figure 3) which demonstrate the presence of higher concentrations of surface oxygen in the more amorphous samples. Either data set alone could be considered as speculative, but together they provide the basis for firm conclusions about the polymer structure and morphology. This is especially important in the case of the ESCA since the present study is a unique demonstration of quantifiable differences in ESCA signal intensities due to different morphological forms of the same homopolymer. Although the information given above provides the basis for spectroscopic characterization, crystallinity measurements are also important. All three results taken together rule out the possibility of spurious effects, such as oxidation, causing the observed changes. It is also important to consider the differences in sampling depths of ESCA and FTIR; greater surface sensitivity of ESCA is one of the key aspects in assessing the chemical ramifications of differing morphologies.

B. Degradation Studies. The calibration studies combined with the degradation studies provide the first direct evidence about the chemical nature of the crystalline and amorphous regions of these well-ordered materials. Also, they demonstrate the higher resistance to chemical attack exhibited by the crystalline core.

This is quantitatively described by the spectroscopic reaction rate studies of Figures 5 and 6 and crystallographically by Figure 7. Examination of the FTIR and SAXS data indicates that HF etching of the single-crystal mat proceeds quickly at first, leveling out as time increases. Both curves in Figure 7 (SAXS) fit well to a $t^{1/2}$ dependence, and assuming a linear fit of the crystal thickness (SAXS) to $t^{1/2}$, where an etching rate of 0.2 Å/min can be derived. This result can be compared to previous results for

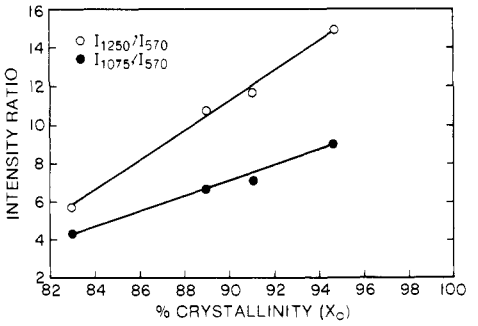

Figure 8. Plot of FTIR relative intensity ratios of vs. degree of crystallinity for etched single-crystal mats (I).

HF solution etching where the rate derived from SAXS analysis was 0.01 Å/min, an order of magnitude lower.[17] The FTIR data in Figure 5 also show linearity when plotted vs. $t^{1/2}$. A combination of data from Figures 5 and 7 is shown in Figure 8, where a linear relationship is derived by plotting FTIR intenstiy ratios vs. crystallinity directly for the etching process on the single crystals.

Examination of the ESCA data serves as another illustration of the difference in sampling depths from FTIR. The etching experiment on the crystal yields ESCA data which plateau before 30 min of etching. This is indicative of both the relatively low level of disordered material in the crystal, which is etched away, and the shallow sampling depth of the technique combining to show a steady state after 15 min of etching. In contrast, ESCA results from the melt cast mats in Figure 6 show continuous linear increases because of the higher concentration of amorphous material in sample II. Both spectroscopic methods thus show changes in relative intensity as crystallinity increases during the chemical etching process. The etching process appears to be very fast for the amorphous material and slower for the crystalline core. Additionally, the complementary use of FTIR and ESCA proved to be very important in deducing the mechanism of the reaction. FTIR evidence showed the growth of Si–OH directly, not easily detectable by ESCA which cannot detect hydrogen.[12,13] ESCA monitored the growth of fluorine, which was not detected by FTIR since bands due to Si–F were masked by the Si–O bands. These data thus provide an extensive chemical and morphological basis for resistance to chemical attack as related to the crystalline structure of this unique material. Work is currently underway, including surface spectroscopic studies by ESCA and SIMS,[14] to further investigate the chemical and morphological basis for differences between crystalline and amorphous regions of polymer systems, which have such an important influence on structure property relationships.

Conclusions

This study has demonstrated a novel use of ESCA to measure differences in surface morphology of a poly(TMpS) homopolymer, manifest throught the use of selective chemical degradation. ESCA and FTIR have been used together successfully to analytically monitor and characterize the changing surface of etched poly(TMpS). These spectroscopic techniques can be employed to monitor the surface chemistry in a way that parallels the crystallinity changes (increase) assessed by DSC and by SAXS measurements. Etching with HF gas, using He diluent, removes the more vulnerable surface material in poly(TMpS) lamellar crystals. In spherulitic specimens the interlamellar regions are more susceptible to chemical attack, degradation also occurring via Si–O–Si chain scission.

Acknowledgment. We acknowledge partial support of this project by the National Science Foundation Polymer (DMR 8113089) and Chemical Analysis (CHE 8108495) Programs.

Registry No. Poly(TMpS), 54811-84-6.

Symmetry Rules for the Determination of the Intercalation Geometry of Host/Guest Systems Using Circular Dichroism: A Symmetry-Adapted Coupled-Oscillator Model

Pieter E. Schipper* and Alison Rodger*

Contribution from the Department of Theoretical Chemistry, The University of Sydney, New South Wales 2006, Australia. *Received June 7, 1982*

Abstract: The intercalation of an achiral guest molecule into a relatively complex chiral host system (e.g., DNA, cyclodextrins) leads to an induced circular dichroism (ICD) of the guest transitions. By exploiting the recently developed generalized selection rules, it is shown that the coupled-oscillator expressions for the guest ICD may be analytically symmetry-adapted for all combinations of host/guest symmetries, leading to a rigorous simplification of the expressions and, more importantly, well-defined conditions under which simple correlations exist relating the ICD sign directly to the intercalation geometry. The results are applied to aromatic guests intercalated into DNA and cyclodextrin hosts, as well as to charge-transfer transitions in chiral metal chelate complexes. Good agreement with experimental results is obtained.

Introduction

The intercalation of aromatic chromophores (guest species) into DNA and cyclic sugars (host species) in aqueous media has been the subject of extensive experimental investigation because of the potential role of intercalation in biological phenomena such as mutagenicity and carcinogenicity.[1-7] Determination of the intercalation geometry by standard X-ray diffraction or NMR methods is virtually precluded by the low concentrations of the intercalated species and the need to study the systems in solution. Such conditions are, however, ideally suited to absorption spectroscopic methods. Linear dichroism (LD) has been used ex-

(1) Kamiya, M. *Biochim. Biophys. Acta* **1979**, *562*, 70, and references therein. (Note that the considerations of this paper are restricted to low adduct concentrations in the DNA case and do not apply to the high concentration limit in which chiral superstructure of the dye are formed.)
(2) Schipper, P. E.; Nordén, B.; Tjerneld, F. *Chem. Phys. Lett.* **1980**, *70*, 17.
(3) Harata, K.; Uedaira, H. *J. Chem. Soc. Jpn.* **1975**, *48*, 375.
(4) Nordén, B. *Appl. Spectrosc. Rev.* **1978**, *14*, 157.
(5) Shimuzu, H.; Kaito, A.; Hatano, M. *Bull. Chem. Soc. Jpn.* **1979**, *52*, 2678; **1981**, *54*, 513.
(6) Yamaguchi, H.; Ikeda, N.; Hirayama, F.; Uekama, K. *Chem. Phys. Lett.* **1978**, *55*, 75.
(7) Ikeda, N.; Yamaguchi, H. *Chem. Phys. Lett.* **1978**, *56*, 167.

0002-7863/83/1505-4541$01.50/0